

RSC Advances



This is an *Accepted Manuscript*, which has been through the Royal Society of Chemistry peer review process and has been accepted for publication.

Accepted Manuscripts are published online shortly after acceptance, before technical editing, formatting and proof reading. Using this free service, authors can make their results available to the community, in citable form, before we publish the edited article. This *Accepted Manuscript* will be replaced by the edited, formatted and paginated article as soon as this is available.

You can find more information about *Accepted Manuscripts* in the [Information for Authors](#).

Please note that technical editing may introduce minor changes to the text and/or graphics, which may alter content. The journal's standard [Terms & Conditions](#) and the [Ethical guidelines](#) still apply. In no event shall the Royal Society of Chemistry be held responsible for any errors or omissions in this *Accepted Manuscript* or any consequences arising from the use of any information it contains.

Cite this: DOI: 10.1039/c0xx00000x

www.rsc.org/xxxxxx

ARTICLE TYPE

Synergetic adsorption and catalytic oxidation performance originated from leafy graphite nanosheets anchored iron(II) phthalocyanine nanorods for efficient organic dye degradation

Guang'en Yuan, Guoquan Zhang*, Yufei Zhou, Fenglin Yang

Received (in XXX, XXX) Xth XXXXXXXXXX 20XX, Accepted Xth XXXXXXXXXX 20XX

DOI: 10.1039/b000000x

Abstract

Leafy graphite nanosheets anchored iron(II) phthalocyanine nanorods (FePc@LGNS) were facilely synthesized without using complex covalent anchoring procedure. FE-SEM, XRD, FTIR, and XPS characterizations confirmed the molecule configuration of FePc on LGNS surface. The interlaced hydrophobic/hydrophilic regions and large specific-surface-area of FePc@LGNS hybrid not only improved the adsorption capacity, but also promoted the oxidative ability of FePc@LGNS-H₂O₂ system due to sufficient FePc catalytic active sites on LGNS surface. The optimal conditions for CR removal were initial pH 6.98, 50 mM H₂O₂ and 1.0 g/L FePc@LGNS hybrid. Different from classical Fenton process, high-valent iron(IV)-oxo complexes and hydroxyl radicals are responsible for Congo red (CR) oxidative degradation. Liquid chromatography-mass spectrometry (LC-MS) analysis demonstrated the effective cleavage of both azo bonds and C-C bonds of CR molecules. The plausible oxidation mechanism of FePc@LGNS-H₂O₂ system and the degradation pathway of CR were proposed. This FePc@LGNS-H₂O₂ system could be a highly efficient oxidation process for recalcitrant pollutants elimination over a wide pH range.

1. Introduction

Metal phthalocyanine (MPc) complexes had been widely used in the oxidative degradation and even mineralization of the recalcitrant pollutants.¹⁻⁴ In the homogeneous MPcS/H₂O₂ systems, the nucleophilic iron-peroxo/oxo complexes other than hydroxyl radicals (•OH) were responsible for the catalytic oxidation.⁵ Moreover, di-iron phthalocyanines like Fe-O-Fe and Fe-N=Fe could be generated by the binuclear macrocyclic complexes.⁶⁻⁹ As an exception, •OH could be generated in FePcS-H₂O₂ system under visible light irradiation.^{2,10} These water-soluble catalysts, however, are difficult to separate from the effluents for reuse, leading to a secondary contamination and catalyst loss.

Anchoring MPc complexes onto the solid supports was an effective strategy to overcome the above drawbacks. Various supporting materials¹¹⁻¹³ were utilized to support MPc complexes through the covalent bonding method. Recently, CoPc was covalently immobilized on some adsorbent materials,¹⁴⁻¹⁷ and these composites possessed high natural affinity to organic

pollutants and exhibited strong H₂O₂-activating ability for organic pollutants degradation. Above-mentioned heterogeneous catalysts had good catalytic activities and stabilities, while the covalent anchoring method generally involves a series of chemical reactions, thus increasing the difficulty of catalyst preparation.

Exfoliated graphite (EG), a kind of porous carbon-based material composed of thin graphite sheets, has been widely used as adsorbent or catalyst support material^{16,18-21} in the field of wastewater treatment. Herein, we reported a simple synthesis method without covalent anchoring to prepare the diagonally accumulative FePc on leafy graphite nanosheets (LGNS) surface, which are composed of mesoporous FePc nanorods structures with the interlaced hydrophobic/hydrophilic regions and large specific surface area. Different characterization techniques were used to investigate the molecular configuration of FePc nanorods upon LGNS surface. The FePc nanorods induced synergy effect between adsorption and the catalytic oxidation of FePc@LGNS hybrid for Congo red (CR)

degradation were investigated in detail in the presence of H_2O_2 over a wide pH range. The intermediate products were analyzed, and the plausible degradation pathway of CR and the catalytic oxidation mechanism of $\text{FePc@LGNS-H}_2\text{O}_2$ system were also proposed.

2. Experimental section

Reagents and materials

Natural flake graphite (600 mesh) was obtained from Shanghai Chemical Reagent Co. FePc was purchased from Tokyo Kasei Co., Japan. Congo red, 30 wt% H_2O_2 and other reagents were of analytical grade and used as received. Deionized water was used throughout the experiments.

Preparation and characterization of the FePc@LGNS hybrid

The FePc@LGNS hybrid was fabricated by a facile acid intercalation-thermal expanding-ultrasonic exfoliation-adsorption/deposition method. The FePc@LGNS hybrid was characterized by means of FE-SEM, XRD, FTIR, XPS and N_2 adsorption/desorption. These details were summarized in *Electronic Supplementary Information (ESI)*.

Adsorption and catalytic oxidation of CR

The details in sorption and catalytic oxidation experiments were summarized in *ESI*. Unless specially stated, the typical experiment conditions were selected as the initial pH 6.98, 30 °C, 1.0 g L^{-1} FePc@LGNS , 50 mM H_2O_2 .

Analysis methods

The decolorization of CR was measured by the spectrophotometric method. The degradation products were analyzed by liquid chromatography-mass spectrometry (LC-MS). Leached iron ion in aqueous solution after catalytic oxidation was detected by atomic absorption spectrophotometer. These details were summarized in *ESI*.

3. Results and discussion

Characterization of catalysts

The acid intercalation and thermal expanding procedure were used to prepare EG with natural flake graphite as the precursor. The volume of graphite was expanded four times approximately (Fig. S1). **Fig. 1a and b** shows that the acid-intercalated graphite and EG exhibit the loosely frizzy morphology, but these lamellas are still compact and parallel to one another with the hierarchical structure. After ultrasonic irradiation (**Fig. 1c**), EG was further split into dispersive LGNS and the inherent frame structures of EG was completely damaged. The FE-SEM images of FePc@LGNS hybrid at different magnifications (**Fig. 1d-f**) display the randomly oriented aggregation of FePc molecules onto LGNS surface, which results in the uniformly distributed nanorod-like morphology with average diameter and length of ~26 and ~250 nm, respectively.

It is reported the FePc molecular preferentially intended to organize with the phthalocyanine ring parallel to the substrate and

aggregate themselves in water and polar solvent by taking advantage of their self-attraction properties between the phthalocyanine molecules.²²⁻²⁴ In terms of the hydrophobic phthalocyanine moieties, a diagonally co-facial stacking would take shape with the increases in solvent polarity and phthalocyanine concentration, due to the stronger directional intermolecular interactions than the molecule-substrate interactions.²⁴ Concerning FePc concentration (0.6 mg/mL) is used, the intermolecular distances of neighboring FePc molecules

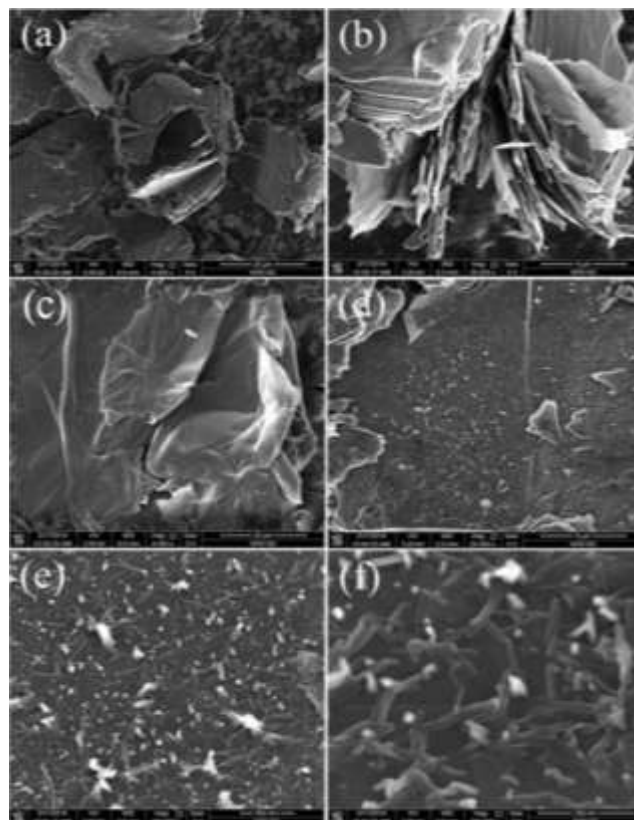


Figure 1. FE-SEM images of (a) acid-intercalated graphite, (b) EG, (c) LGNS, (d-f) FePc@LGNS hybrid at different magnifications.

could decrease substantially. Thus, the directional FePc-FePc intermolecular interactions become predominant compared to FePc-LGNS molecule-substrate interactions, which assemble FePc molecules into short chains and even into distinctive nanorod configurations. Previous reports²⁴ inspire the authors to speculate the FePc nanorod structure, similar to F16CuPc nanoribbon, as depicted in Fig. S2. The FePc molecules are stacked along the diagonal growth direction, in the meanwhile, the coordination reaction between six N atoms and one Fe atom and the $\pi-\pi$ interactions between FePc molecules could firmly hold FePc molecules together. Such molecular organization will further verified by FTIR and XPS characterizations.

The XRD patterns of FePc , Graphite, LGNS and FePc@LGNS hybrid are shown in **Fig. 2a**. The diffraction peaks of FePc powder located at 6.8° , 15.5° and 24.9° correspond respectively to the lattice spacing of 13.0, 5.7 and 3.6 Å.²⁵ In other three patterns, the peaks centered at ca. 26.4° , 44.4° and 54.5° can be indexed respectively to the (002), (101) and (004) planes of graphite

crystal.^{25,26} The amplified XRD patterns in 22–30° are displayed in Fig. S3. Apparently, no remarkable difference in G(002) peak was observed in other three samples as previously reported,²¹ suggesting no variation in the nanoscale lamellae structure after the expansion and exfoliation of graphite. To clearly distinguish the diffraction peak of (002) plane of FePc in FePc@LGNS hybrid, XRD patterns in 4–20° were extracted. As seen in Fig. 2b, the FePc@LGNS hybrid possesses two intensive peaks similar to pure FePc, and an additional peak located at ca. 13.8°, agreeing well with the status that FePc was anchored on graphene sheets through the π - π stacking interaction²⁷ and further demonstrating the successful loading of FePc on LGNS surface.

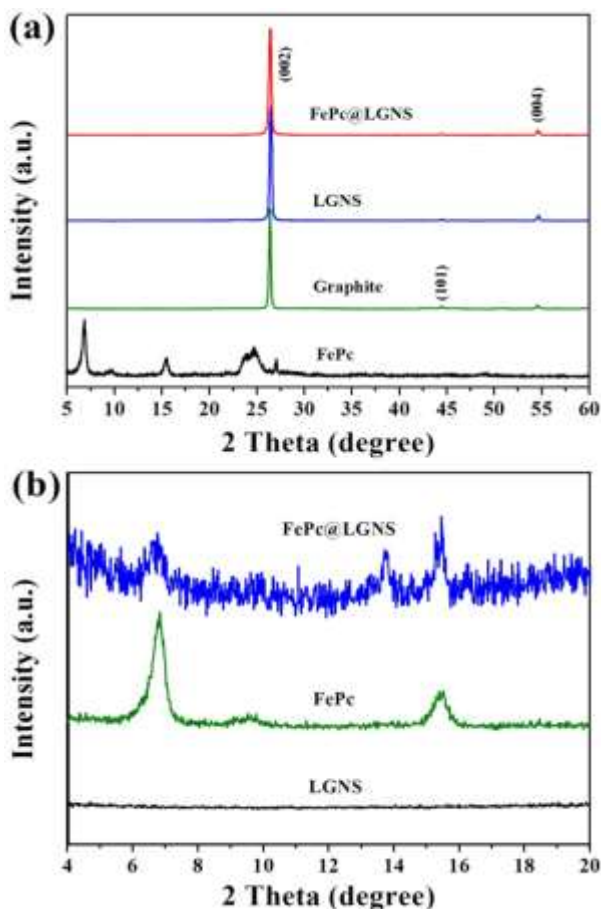


Fig. 2. (a) XRD patterns of FePc, Graphite, LGNS and FePc@LGNS hybrid; (b) XRD patterns in the angular range of 4–20°.

Fig. 3a shows the survey XPS patterns of Graphite, LGNS, FePc@Graphite and FePc@LGNS hybrids. The relative atomic percentages are summarized in Table 1.

Table 1. The relative atomic percentages of C, O, N and Fe elements in various samples.

Samples	C (at. %)	O (at. %)	N (at. %)	Fe (at. %)
Graphite	94.54	5.46	—	—
LGNS	88.66	11.34	—	—
FePc@Graphite	91.43	8.30	0.22	0.05
FePc@LGNS	89.27	6.79	3.36	0.58

Obviously, Graphite and LGNS samples are mainly composed of carbon (284.6 eV) and oxygen (532.8 eV) atoms. After the acid-intercalated oxidation, the C/O ratio of LGNS (17.33) are much higher than that of Graphite (7.82). As to the FePc@Graphite hybrid, a weak peak centered at ca. 398.6 eV was observed, which are assigned to nitrogen atoms of FePc.²⁸ In comparison, XPS spectrum of FePc@LGNS hybrid shows much more intensive N 1s peak and Fe 2p peak. According to the relative atom percentages of Fe, more than 10 times of FePc molecules was supported on LGNS compared to commercial Graphite, which is due mainly to the large specific surface area of LGNS, as described latter in BET measures. Fig. 3b–d shows the high resolution XPS patterns of O 1s, N 1s and Fe 2p of the FePc@LGNS hybrid, respectively. The O 1s spectra can be

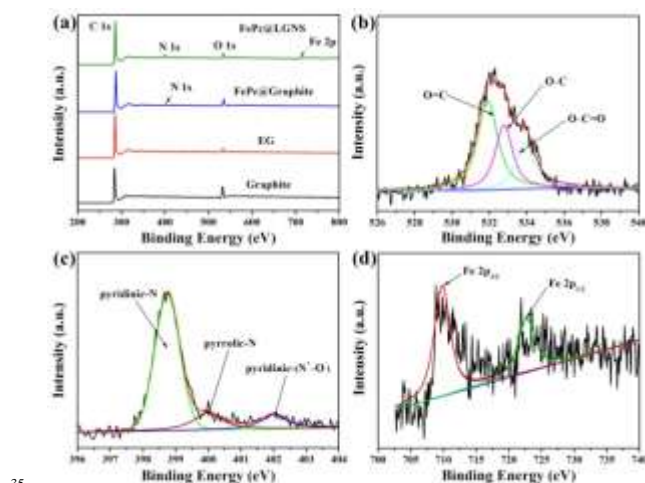


Fig. 3. (a) XPS survey scan of Graphite, LGNS, FePc@Graphite and FePc@LGNS hybrids; High resolution XPS spectra of (b) O 1s, (c) N 1s, and (d) Fe 2p of the FePc@LGNS hybrid.

divided into three peaks at 531.8, 532.7 and 533.9 eV with the relative intensity ratio of 1.84:1.34:1, which belong respectively to C=O, C–O and O–C=O groups.²⁹ The N 1s spectrum also consists of three components, which are attributed to pyridinic-N (398.8 eV), pyrrolic-N (400.0 eV) and oxidized N (402.0 eV).³⁰ The pyridinic-N peak accounts for ~74.2%, corresponding to N atoms coordinating with Fe atoms, while the other two peaks account only for ~14.7% and ~11.1%, respectively. This result implies that about three quarters of N atoms are coordinated with Fe. The Fe 2p spectrum can be divided into two main peaks at 709.8 and 722.7 eV with the relative intensity ratio of 2:1, which are assigned respectively to Fe 2p_{3/2} and Fe 2p_{1/2} asymmetric}

bands.^{31,32} Additionally, the spin splitting interval of Fe ($2p_{1/2} - 2p_{3/2}$) was 12.9 eV, indicating the paramagnetic high-spin Fe(II) in FePc@LGNS hybrid. This result is consistent with the presumed structure of FePc nanorods, in which three quarters of N atoms are coordinated with Fe.

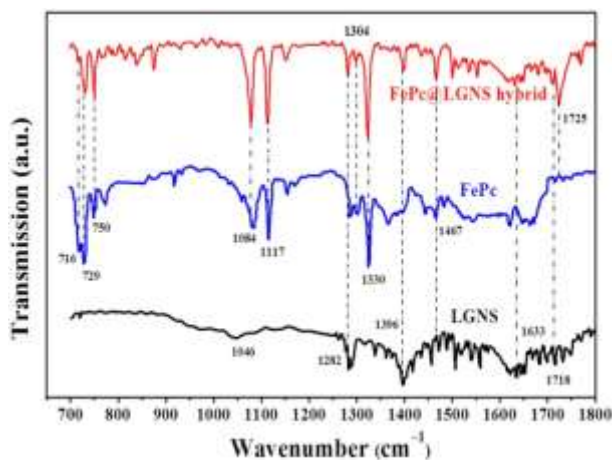
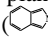


Fig. 4. FTIR spectra in the transmission mode for LGNS, FePc and FePc@LGNS hybrid.

Fig. 4 shows the FTIR spectra of LGNS, FePc and FePc@LGNS hybrid. The spectrum of LGNS exhibits typical stretching vibration peaks at $\sim 1046\text{ cm}^{-1}$ for C–OH and $\sim 1282\text{ cm}^{-1}$ for C–O–C.³³ The =C–O stretching vibration of carboxyl group and –OH bending vibration of the combinative water on LGNS surface are located at ~ 1396 and $\sim 1633\text{ cm}^{-1}$, respectively.^{21,33,34} The characteristic peak at $\sim 1718\text{ cm}^{-1}$ comes from the limbic C=O stretching of carbonyl group.³⁴ The FTIR spectrum of FePc powders on KBr pallet is characterized by the strong bands at $\sim 729\text{ cm}^{-1}$ for C–H out-of-plane bending vibration and 750 cm^{-1} for benzene and isoindole () in-plane deformation and Fe–N stretching.^{22,23} The bands of 1084, 1117 and 1304 cm^{-1} are attributed to C–N stretching, Fe–N of pyrrole and C–H in-plane bending vibrations, and 1330 cm^{-1} and 1467 cm^{-1} are assigned to C=C or C=N stretching of pyrrole ring and isoindole stretching in the plane of FePc macrocycle, respectively.^{35,36} The above bands are also detected in FTIR spectrum of FePc@LGNS hybrid in addition to a new band at 1725 cm^{-1} , which is attributed to Fe–N metal-axial ligands of the diagonally stacked FePc molecules on LGNS surface.²²

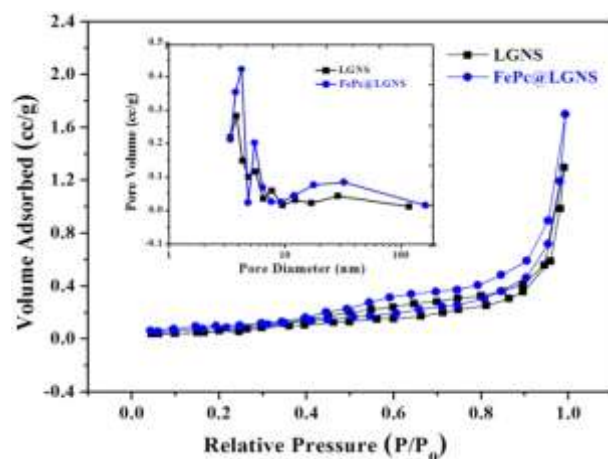


Fig. 5. N_2 adsorption-desorption isotherms of LGNS and FePc@LGNS hybrid. The inset shows the pore size distribution curve obtained from the desorption branch through the BJH method.

N_2 adsorption-desorption isotherms of LGNS and FePc@LGNS hybrid are shown in **Fig. 5**. A little difference in typical type IV isotherms indicated the similar structures and adsorption properties of the two samples. Additionally, distinct type H3 hysteresis loops were observed in the large relative pressure (P/P_0) range of 0.4–1.0, demonstrating the presence of hierarchical porosity and split materials. The dramatic increase in the adsorbed volumes at P/P_0 from 0.9 to 1.0 indicates the occurrence of capillary condensation during the adsorption process.^{21,37} The measured BET surface areas of LGNS and FePc@LGNS samples were 39.3 and $64.8\text{ m}^2\text{ g}^{-1}$, respectively. The pore distribution of LGNS and FePc@LGNS samples in inset of **Fig. 5** showed that most of the pores concentrate upon the range from 3.7 to 15.3 nm, indicating the typical mesoporous structure of LGNS and FePc@LGNS samples. Undoubtedly, such porous structure provides efficient transport pathways for CR molecules to diffuse into the interior pore cavities, which would improve their removal efficiencies by FePc@LGNS- H_2O_2 system.

CR removal through adsorption and catalytic oxidation

Fig. 6a shows the change in CR decolorization rate under different experimental conditions. Obviously, CR removal is almost negligible by H_2O_2 . Although the FePc- H_2O_2 system is just like a classic Fenton process, only $\sim 21.5\%$ CR was removed

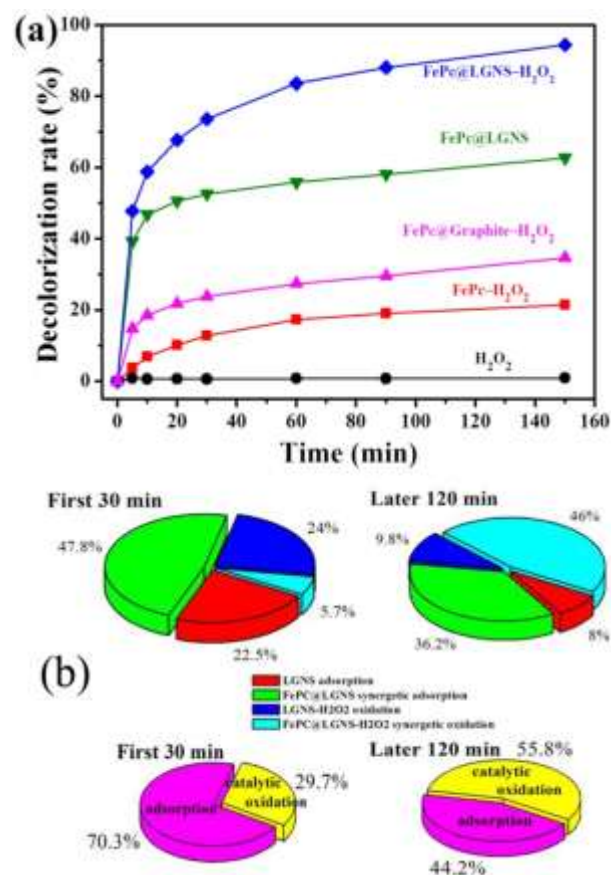


Fig. 6. (a) Time-course evolution of CR decolorization rate under different conditions. (Conditions: pH 6.98, 50 mM H₂O₂, the concentrations of FePc, FePc@LGNS and FePc@Graphite are 1.0 g/L), (b) the contribution ratios of different process in CR elimination at different time periods.

within 150 min, which is attributed to the water insoluble and easy self-aggregate property of FePc in neutral medium,²²⁻²⁴ thus decreasing its catalytic activity. In the case of only FePc@LGNS hybrid, the decolorization rate increased rapidly and ~50.6% CR was eliminated within 30 min, indicating the superior adsorption capacity of FePc@LGNS hybrid. However, the additional control experiments with LGNS and LGNS-H₂O₂ (Fig. S4) showed that CR elimination exhibits a nearly identical tendency in the two cases, which achieve only ~18% and ~19.5% CR decay, respectively. Previous studies³⁷ suggested that although carbon-based heterogeneous catalysts can efficiently activate H₂O₂ molecule producing reactive oxygen species, the contribution of the direct catalysis mediated by the unmodified carbon materials was generally insignificant. Accordingly, CR decay in Fig. S4 should be attributed mainly to the adsorption roles of LGNS.

Except for the carbon atom layers, exfoliated graphite oxide nanosheets possess many hydrophilic oxygen-containing groups.^{21,30} Thus, an interlaced nanostructure containing the hydrophobic FePc and hydrophilic LGNS regions would form on FePc@LGNS hybrid surface. Compared to the adsorption performance of LGNS, the synergistic effect between FePc nanorods and LGNS causes the enhanced adsorption capacity of FePc@LGNS hybrid towards CR molecules containing both the

hydrophobic and hydrophilic groups,³⁸ where FePc nanorods play an important role in the adsorption process.

CR degradation through FePc@LGNS-H₂O₂ and FePc@Graphite-H₂O₂ systems was carried out for the purpose of comparison. A significant CR elimination with a ~94.4% decolorization rate was achieved in FePc@LGNS-H₂O₂ system after 150 min reaction, which is much more efficient than the FePc@Graphite-H₂O₂ system. The higher CR decolorization percentage in the former case may be ascribed to the higher content of FePc (as demonstrated in Table 1) on the high-specific-surface-area LGNS, which provide larger quantity of active sites for the formation of strong oxidizing species and, equally important, for CR adsorption. In this context, the poor performance of the FePc@Graphite-H₂O₂ system towards CR elimination is due mainly to the large size, low porosity and low surface area of the commercial Graphite powders.

According to the results shown in Fig. 6a, we can easily quantify the contribution proportions of adsorption and catalytic oxidation of the FePc@LGNS-H₂O₂ system towards CR removal. As observed, ~50.6% CR was removed through the adsorption process, whereas ~72% CR was eliminated during the first 30 min. Therefore, the adsorption of FePc@LGNS hybrid is ~70.3% and the catalytic oxidation is ~29.7%. In latter 120 min, ~12.1% and ~22.4% CR was respectively removed by adsorption and catalytic oxidation, thus CR elimination attributed to catalytic oxidation grows to ~55.8%. The contribution percentages of adsorption and catalytic oxidation toward CR elimination at different time regions was depicted in Fig. 6b, in which the detailed contribution rates of adsorption and catalytic oxidation regarding to sole LGNS and FePc@LGNS hybrid were also given. Above results confirmed that FePc nanorods play important roles toward CR removal, which not only facilitate the adsorption capacity of FePc@LGNS hybrid, but also promote the oxidative ability of FePc@LGNS-H₂O₂ system, indicating the excellent synergistic effect in FePc@LGNS-H₂O₂ system.

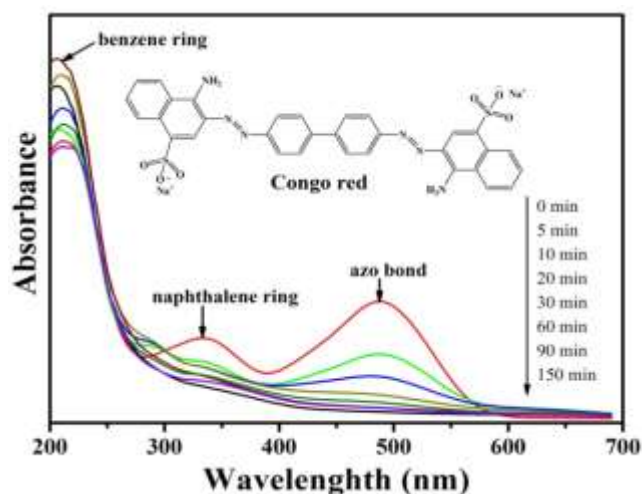


Fig. 7. UV-visible spectrum change of CR during FePc@LGNS-H₂O₂ process. (Conditions: pH 6.98, 1.0 g L⁻¹ FePc@LGNS, and 50 mM H₂O₂).

The change in UV-visible spectrum during FePc@LGNS-

H₂O₂ oxidation process was depicted in Fig. 7. The original CR spectrum exhibited three peaks at 212, 332 and 488 nm, which are attributed respectively to benzene ring, naphthalene ring and azo bond of CR molecule.³⁹ The absorption peak at 488 nm decreases rapidly and disappears nearly at 150 min, indicating the complete cleavage of azo bonds. In the meanwhile, the peak at 332 nm also drops to a certain level, while the 212 nm peak increases to the maximum value at 60 min and gradually declines afterwards. These findings demonstrate that the naphthalene ring of CR was cleaved into benzene derivatives first, and then transformed into non-aromatic organics.

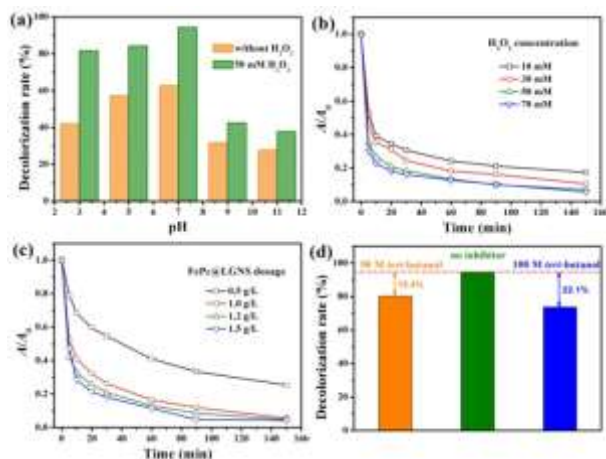


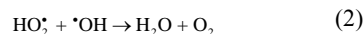
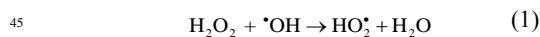
Fig. 8. Effects of (a) initial solution pH, (b) H₂O₂ concentration, (c) FePc@LGNS hybrid dosage and (d) *tert*-butanol dosages on CR decolorization during FePc@LGNS–H₂O₂ process within 150 min. Conditions: (a) 1.0 g L⁻¹ FePc@LGNS, (b) pH 6.98, 1.0 g L⁻¹ FePc@LGNS, (c) pH 6.98, 50 mM H₂O₂ and (d) pH 6.98, 1.0 g L⁻¹ FePc@LGNS, 50 mM H₂O₂.

Influencing factor on FePc@LGNS–H₂O₂ system

The initial solution pH had great impacts on both adsorption and the catalytic activity of heterogeneous catalysts. As shown in Fig. 8a, the adsorption capacity of FePc@LGNS hybrid in neutral solution is higher than that in acidic and alkaline media, which is different from other reports.^{37,38,40} It should be noted that the chemical polarity of CR molecule is strongly affected by the solution pH. CR is negatively charged at pH > 5.5, while it is positively charged at pH below 5.5.⁴⁰ The pH of the point of zero charge (pH_{PZC}) of FePc@LGNS hybrid was measured as 2.9 (Fig. S5). After adding 1.0 g/L FePc@LGNS hybrid, pH value declined obviously from the initial 6.98 to 5.8, which is closed to the pH_{PZC} of CR molecule, resulting in the highest adsorption capacity towards CR. On the other hand, the FePc@LGNS–H₂O₂ system exhibited excellent oxidative ability in the pH range from 3.0 to 7.0, however, the decolorization rate decreases in the alkaline media due to the non-contributive H₂O₂ decomposition. Thus, the proposed FePc@LGNS–H₂O₂ system could be a promising candidate as potential advanced oxidation process for organic wastewater treatment under acidic or neutral media.

Effects of H₂O₂ dosage on CR removal were investigated in the range of 10–70 mM at pH 6.98. As shown in Fig. 8b, the decolorization rate increases with the increasing H₂O₂ concentration, which is different from the classic Fenton process

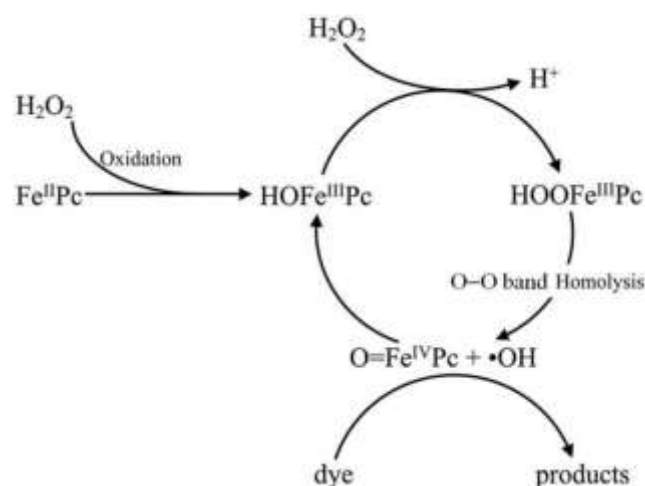
that excess amount of H₂O₂ would consume [•]OH via the following side reactions:



This extraordinary phenomenon implied the occurrence of other strong oxidizing species in addition to hydroxyl radical, which will be discussed below.

Effect of FePc@LGNS dosage on CR removal was examined ranging from 0.5 to 1.5 g/L. As seen in Fig. 8c, CR decolorization rate increases rapidly when FePc@LGNS dosage increased from 0.5 to 1.5 g/L, which is due mainly to the enhanced adsorption of CR and the increasing amount of active sites on FePc@LGNS surface for the formation of strong oxidizing species toward CR degradation.

Tert-butanol can be used to verify the presence of [•]OH during the course of oxidation.⁴¹ As shown in Fig. 8d, CR decolorization rate decreases to ~80.0% in the presence of 50 mM *tert*-butanol, implying the involvement of [•]OH in FePc@LGNS–H₂O₂ system. Theoretically, all [•]OH produced by 50 mM H₂O₂ and iron catalyst could be consumed by 50 mM *tert*-butanol. However, ~73.5% CR was still removed within 150 min in the presence of 100 mM *tert*-butanol, which is 1.17 times as much that achieved only by FePc@LGNS hybrid adsorption. Result indicated that the addition of *tert*-butanol leads to a certain extent decrease in CR elimination, but the FePc@LGNS–H₂O₂ system still possesses considerable oxidative ability in the presence of excessive *tert*-butanol. Therefore, a kind of strong oxidizing species that is more dominant than [•]OH must be involved in FePc@LGNS–H₂O₂ system.



Scheme 1. Proposed catalytic oxidation mechanism of the FePc@LGNS–H₂O₂ system.

From the characterization data, it is obvious that no di-iron phthalocyanines were formed in the synthesis process of FePc@LGNS hybrid. Therefore, the role of FePc nanorods in oxidation process should similar to mononuclear iron complexes. Previous research^{5,15,17,42–45} reported that the iron-oxygen

complexes (iron(III)-peroxo/oxo) were considered as the active intermediates in MPC-H₂O₂ systems. Iron(III)-peroxo complexes could be easily converted into iron(III)-hydroperoxo complexes via protonation, followed by generating high-valent iron(IV)-oxo complexes and •OH radicals via homolysis of O–O bonds.^{46,47} In present work, the π–electron reactions are widely exist between FePc molecules, which can undoubtedly promote the homolysis

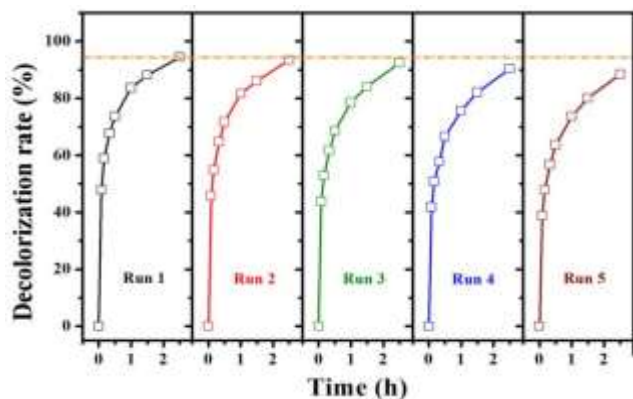


Fig. 9. The stability of FePc@LGNS hybrid in five consecutive runs. (Conditions: pH 6.98, 50 mM H₂O₂, 1.0 g/L FePc@LGNS hybrid, and 0.1 mM CR).

of O–O bonds. As seen in Scheme 1, the FePc molecules are first oxidized by H₂O₂ and then transformed into aquo complexes (HOFe^{III}Pc) via coordination reaction with OH[−]. Subsequently, H₂O₂ molecules replace OH[−] to give iron(III)-hydroperoxo complexes (HOOFc^{III}Pc) due to its nucleophilic nature.^{42,44} The O–O bonds of these iron(III)-hydroperoxo complexes are symmetrically cleaved into iron(IV)-oxo complexes (O=Fe^{IV}Pc) and •OH radicals. Finally, iron(IV)-oxo complexes are reduced back to aquo complexes and then step into the next cycle.

The catalytic stability of FePc@LGNS hybrid was evaluated by five consecutive cycles under the typical conditions of pH 6.98, 1.0 g L^{−1} FePc@LGNS, and 50 mM H₂O₂. As seen from **Fig. 9**, the catalytic activity of FePc@LGNS hybrid is reduced by only 6.0% after five runs. No free iron ions were detected in the aqueous phase, indicating that the catalytic activity was primarily attributed to the heterogeneous FePc@LGNS catalyst and not the homogeneous dissolved iron ions. The slight decrease in CR decolorization rate may be resulted from the loss of small amount of FePc@LGNS hybrid during the separation and transformation.

Product analysis and possible degradation pathway of CR

Detection of degradation intermediates was essential for explaining and understanding the mechanisms of FePc@LGNS–H₂O₂ oxidation system. The intermediate products identified by LC–MS are summarized in **Table 2** and their ESI mass spectra are shown in Fig. S6. Obviously, most of the intermediate products are benzenic compounds and no fragmentary products containing azo bonds were found. The presence of M₁ suggests the symmetrical cleavage of azo bonds of CR. The products of M₁₀ and M₁₁ may originate from the symmetrical cleavage of two benzene rings of CR molecule, while other aromatic compounds may be the oxidative products of M₁. These results indicate that

both azo bonds and aromatic ring structures of CR were destructed, which agrees well with the UV-vis spectroscopy results.

The plausible degradation pathway of CR is proposed in **Fig. 10**. A CR molecule was first decomposed into M₁ and *p*-nitrophenol (not detected) through symmetrical cleavage of azo bonds and two benzene rings of CR. The naphthalene ring of M₁ was cleaved via three ways, forming M₂, M₃, or M₅ and M₆. Compound M₁ was converted into M₄ through denitration. Decarboxylation of M₂ generated M₃, followed by hydroxylation

Table 2. The detected intermediate products during CR oxidative degradation by FePc@LGNS-H₂O₂ system

Fragment	Molecular formula	m/z	Proposed structure
M ₁₀	C ₆ H ₆ O	93	
M ₂	C ₉ H ₈ O ₅	97, 195	
M ₆	C ₃ H ₄ O ₄	103	
M ₁₂	C ₄ H ₄ O ₄	115	
M ₉	C ₇ H ₆ O ₃	137	
M ₁₁	C ₆ H ₆ O ₄	141	
M ₈	C ₃ H ₈ O ₃ S	155	
M ₃	C ₈ H ₆ O ₄	165	
M ₇	C ₈ H ₆ O ₅	95, 181	
M ₄	C ₁₀ H ₇ O ₄ S	223	
M ₅	C ₈ H ₅ NO ₇	227	
M ₁	C ₁₀ H ₆ N ₂ O ₇ S	297	

to M₇. Compound M₄ was cleaved into M₈ and M₉ or transformed into M₃, depending on the breaking position of naphthalene ring. Compound *p*-nitrophenol could be oxidized to M₁₀ or M₁₁

through denitration, and the hydroxylation of M₁₀ can also generate M₁₁. The above benzenic compounds obtained were subsequently transformed into M₅, M₁₂ or other organic acids through benzene ring opening.

10 Conclusions

FePc@LGNS hybrid was prepared through a simple synthesis

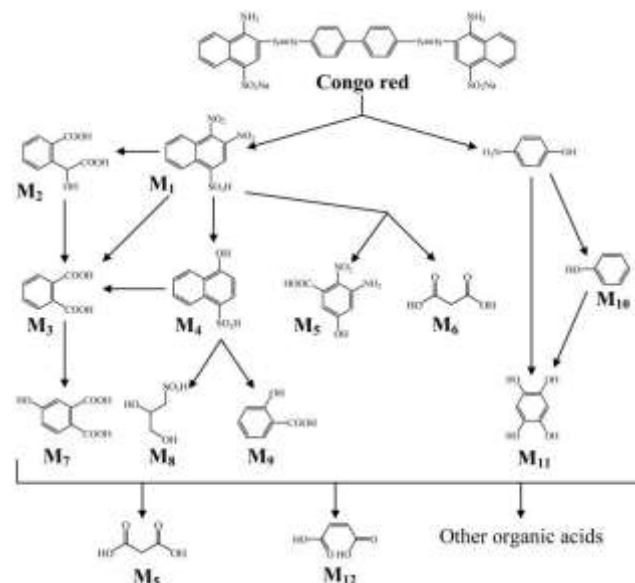


Fig. 10. Possible degradation pathway of CR via the FePc@LGNS-H₂O₂ system.

15 method without covalent anchoring procedure. Characterization data exhibited that the diagonal stacking of FePc resulted in the mesoporous FePc nanorod structure, which was uniformly distributed on LGNS surface. The excellent synergistic effect between the hydrophobic FePc nanorods and the hydrophilic
20 LGNS improved the adsorption capacity of FePc@LGNS hybrid and consequently promoted the oxidative degradation of CR in the developed FePc@LGNS-H₂O₂ system. A decolorization rate of 94.4% was achieved within 150 min in neutral solution. The high-valent iron(IV)-oxo complexes and •OH radicals are
25 responsible for CR oxidative degradation, resulting in the efficient cleavage of azo bonds and C–C bonds of aromatic ring of CR. The catalytic activity of FePc@LGNS hybrid was reduced by only 6.0% after five runs. Thus, the FePc@LGNS-H₂O₂ system could be a promising candidate as potential advanced
30 oxidation process for refractory contaminants treatments due to its admirable synchronous role of coupled adsorption and catalytic oxidation. More importantly, the proposed synthesis strategy can be extended to fabricate other high-performance catalysts based on nano-carbon materials in advanced oxidation
35 process for wastewater treatment.

Acknowledgements

The authors would like to acknowledge the National Natural Science Foundation (No.21177017) and the Fundamental Research Funds for the Central Universities (No.DUT13LK50)
40 for their financial support.

Notes and references

Key Laboratory of Industrial Ecology and Environmental Engineering, Ministry of Education, School of Environmental Science and Technology, Dalian University of Technology, Dalian 116023, China. Fax: +86-411-84706328; Tel: +86-411-84706328; E-mail: guoquanz@126.com

† Electronic Supplementary Information (ESI) available: [Preparation and characterization of FePc@LGNS Hybrid, crystal structure of FePc nanorods, XRD patterns in the angular range of 22–30°, ESI mass spectra and the detected intermediate products during CR degradation by FePc@LGNS-H₂O₂ system]. See DOI: 10.1039/b000000x/.

- 1 A.B. Sorokin, *Chem. Rev.*, 2013, **113**, 8152–8191.
- 2 X. Tao, W. Ma, T. Zhang, J. Zhao, *Chem. Eur. J.*, 2002, **8**, 1321–1326.
- 3 A. Sorokin, B. Meunier, J. Séris, *Science*, 1995, **268**, 1163–1166.
- 4 A. Sorokin, S. De Suzzoni-Dezard, D. Poullain, J.-P. Noël, B. Meunier, *J. Am. Chem. Soc.*, 1996, **118**, 7410–7411.
- 5 A. Sorokin, B. Meunier, *Chem. Eur. J.*, 1996, **2**, 1308–1317.
- 6 E. Viola, F. Monacelli, *J. Porphyr. Phthalocya.*, 2006, **10**, 13–21.
- 7 E.V. Kudrik, A.B. Sorokin, *Chem. Eur. J.*, 2008, **14**, 7123–7126.
- 8 L.X. Alvarez, E.V. Kudrik, A.B. Sorokin, *Chem. Eur. J.*, 2011, **17**, 9298–9301.
- 9 P. Afanasiev, E.V. Kudrik, J.M. Millet, D. Bouchu, A.B. Sorokin, *Dalton Trans.*, 2011, **40**, 701–710.
- 10 X. Tao, W. Ma, T. Zhang, J. Zhao, *Angew. Chem. Int. Ed.*, 2001, **40**, 3014–3016.
- 11 A.B. Sorokin, A. Tuel, *Catal. Today*, 2000, **57**, 45–59.
- 12 P. Ratnasamy, D. Srinivas, *Catal. Today*, 2009, **141**, 3–11.
- 13 C. Shen, S. Song, L. Zang, X. Kang, Y. Wen, W. Liu, L. Fu, *J. Hazard. Mater.*, 2010, **177**, 560–566.
- 14 W. Chen, W. Lu, Y. Yao, M. Xu, *Environ. Sci. Technol.*, 2007, **41**, 6240–6245.
- 15 W. Lu, W. Chen, N. Li, M. Xu, Y. Yao, *Appl. Catal. B*, 2009, **87**, 146–151.
- 16 W. Lu, N. Li, W. Chen, Y. Yao, *Carbon*, 2009, **47**, 3337–3345.
- 17 W. Lu, N. Li, S. Bao, W. Chen, Y. Yao, *Carbon*, 2011, **49**, 1699–1709.
- 18 F. Vieira, I. Cisneros, N.G. Rosa, G.M. Trindade, N.D.S. Mohallem, *Carbon*, 2006, **44**, 2590–2592.
- 19 W. Li, C. Han, W. Liu, M. Zhang, K. Tao, *Catal. Today*, 2007, **125**, 278–281.
- 20 I.M. Afanasov, O.N. Shornikova, V.V. Avdeev, O.I. Lebedev, G.V. Tendeloo, A.T. Matveev, *Carbon*, 2009, **47**, 513–518.
- 21 G. Chen, W. Weng, D. Wu, C. Wu, J. Lu, P. Wang, X. Chen, *Carbon*, 2004, **42**, 753–759.
- 22 P. Alessio, M.L. Rodriguez-Mendez, J.A. De Saja Saez, C.J. Constantino, *Phys. Chem. Chem. Phys.*, 2010, **12**, 3972–3983.
- 23 V. Zucolotto, M. Ferreira, M.R. Cordeiro, C.J.L. Constantino, D.T. Balogh, A.R. Zanatta, W.C. Moreira, O.N. Oliveira, *J. Phys. Chem. B*, 2003, **107**, 3733–3737.
- 24 S.M. Yoon, H.J. Song, I.-C. Hwang, K.S. Kim, H.C. Choi, *Chem. Commun.*, 2010, **46**, 231–233.
- 25 M. Mahyari, A. Shaabani, *Appl. Catal. A*, 2014, **469**, 524–531.
- 26 A. Yasmin, J.-J. Luo, I.M. Daniel, *Compos. Sci. Technol.*, 2006, **66**, 1182–1189.
- 27 C. Zhang, R. Hao, H. Yin, F. Liu, Y. Hou, *Nanoscale*, 2012, **4**, 7326–7329.
- 28 R.L. Arechederra, K. Artyushkova, P. Atanassov, S.D. Minteer, *ACS Appl. Mater. Inter.*, 2010, **2**, 3295–3302.
- 29 H. Yan, X. Tao, Z. Yang, K. Li, H. Yang, A.M. Li, R.S. Cheng, *J. Hazard. Mater.*, 2014, **268**, 191–198.
- 30 L. Sun, H.W. Yu, B. Fugetsu, *J. Hazard. Mater.*, 2012, **203–204**, 101–110.
- 31 Q. Cui, S. Chao, P. Wang, Z. Bai, H. Yan, K. Wang, L. Yang, *RSC Adv.*, 2014, **4**, 12168–12174.
- 32 A. Velázquez-Palenzuela, L. Zhang, L. Wang, P.L.s. Cabot, E. Brillas, K. Tsay, J. Zhang, *J. Phys. Chem. C*, 2011, **115**, 12929–12940.
- 33 Z.-L. Chen, F.-Y. Kam, R.G.S. Goh, J. Song, G.-K. Lim, L.-L. Chua, *Chem. Mater.*, 2013, **25**, 2944–2949.
- 34 D.W. Lee, J.W. Seo, *J. Phys. Chem. C*, 2011, **115**, 12483–12486.
- 35 P. Bertoncello, M. Peruffo, *Colloids Surfaces A*, 2008, **321**, 106–112.
- 36 D. Volpati, P. Alessio, A.A. Zanolim, F.C. Storti, A.E. Job, M. Ferreira, A. Riul, O.N. Oliveira, C.J.L. Constantino, *J. Phys. Chem. B*, 2008, **112**, 15275–15282.
- 37 X. Hu, B. Liu, Y. Deng, H. Chen, S. Luo, C. Sun, P. Yang, S. Yang, *Appl. Catal. B*, 2011, **107**, 274–283.
- 38 L. Torkian, B.G. Ashtiani, E. Amereh, N. Mohammadi, *Desalin. Water Treat.*, 2012, **44**, 118–127.
- 39 J.-S. Chang, C. Chou, Y.-C. Lin, P.-J. Lin, J.-Y. Ho, T. Lee Hu, *Water Res.*, 2001, **35**, 2841–2850.
- 40 M.K. Purkait, A. Maiti, S. DasGupta, S. De, *J. Hazard. Mater.*, 2007, **145**, 287–295.
- 41 C. Jiang, S. Pang, F. Ouyang, J. Ma, J. Jiang, *J. Hazard. Mater.*, 2010, **174**, 813–817.
- 42 F. Li, K.K. Meier, M.A. Cranswick, M. Chakrabarti, K.M. Van Heuvelen, E. Munck, L. Que, *J. Am. Chem. Soc.*, 2011, **133**, 7256–7259.
- 43 E.I. Solomon, S.D. Wong, L.V. Liu, A. Decker, M.S. Chow, *Curr. Opin. Chem. Boil.*, 2009, **13**, 99–113.
- 44 A. Franke, C. Fertinger, R. van Eldik, *Chem. Eur. J.*, 2012, **18**, 6935–6949.

-
- 45 J.-G. Liu, T. Ohta, S. Yamaguchi, T. Ogura, S. Sakamoto, Y. Maeda, Y. Naruta, *Angew. Chem., Int. Ed.*, 2009, **121**, 9426-9431.
- 46 L.V. Liu, S. Hong, J. Cho, W. Nam, E.I. Solomon, *J. Am. Chem. Soc.*, 2013, **135**, 3286-3299.
- 5 47 J. Cho, S. Jeon, S.A. Wilson, L.V. Liu, E.A. Kang, J.J. Braymer, M.H. Lim, B. Hedman, K.O. Hodgson, J.S. Valentine, E.I. Solomon, W. Nam, *Nature*, 2011, **478**, 502-505.